Histone H2A variants enhance the initiation of base excision repair in nucleosomes

Chuxuan Li and Sarah Delaney*

Department of Chemistry, Brown University, 324 Brook Street, Providence, RI 02912, United States

E-mail: delaney@brown.edu
Phone: +1 4018633590. Fax: +1 4018632594

Abstract

Substituting histone variants for their canonical counterparts can profoundly alter chromatin structure, thereby impacting multiple biological processes. Here, we investigate the influence of histone variants from the H2A family on excision of uracil (U) by the base excision repair (BER) enzymes uracil DNA glycosylase (UDG) and single-strand selective monofunctional uracil DNA glycosylase (SMUG1). Using a DNA population with globally distributed U:G bp, enhanced excision is observed in H2A.Z and macroH2A-containing nucleosome core particles (NCPs). The U with reduced solution accessibility exhibit limited UDG activity in canonical NCPs but are more readily excised in variant NCPs, reflecting the ability of these variants to facilitate excision at sites that are otherwise poorly repaired. We also find that U with the largest increase in excision in variant NCPs are clustered in regions with differential structural features between the variants and canonical H2A. Within 35-40 bp from the DNA terminus in macroH2A NCPs, the activities of both glycosylases are comparable to that on free duplex. We show that this high level of activity results from two distinct species within the macroH2A NCP ensemble: octasomes and hexasomes. These observations reveal potential functions for H2A variants in promoting BER and preventing mutagenesis within the context of chromatin.

Introduction

As cellular DNA is constantly exposed to damaging agents from both endogenous and exogenous sources, DNA repair is vital for maintaining genomic integrity and preventing mutagenesis (*1*). Detrimental chemical modification of nucleobases is repaired via the base excision repair (BER) pathway. A DNA glycosylase enzyme initiates BER by recognizing its lesion substrate and cleaving the glycosidic bond, generating an abasic site, and the repair event is completed by downstream BER enzymes (*2*, *3*).

Uracil (U) is one of the most prevalent nucleobase lesions in DNA (*4*). It can result from either misincorporation of dUMP opposite A during replication or spontaneous cytosine deamination, with the latter giving rise to U:G base pairs (bp). Spontaneous cytosine deamination is estimated to occur at a rate of 100-500 events per cell per day (*4*). It was recently reported that U accumulation in CpG sites arises primarily from cytosine deamination in mice lacking the two major glycosylases responsible for excising U from U:G bp (*5*–*7*), uracil DNA glycosylase (UDG) and single-strand selective monofunctional uracil DNA glycosylase (SMUG1) (*8*). If left unrepaired, U:G bp lead to C to T substitutions, which are the most common mutational signatures in human cancer (*9*). Compared with UDG, SMUG1 excises U opposite G less efficiently and has been suggested as a backup for UDG but with broader substrate

specificity (*6*, *10*). It is known that the highest levels of UDG are present during S phase and that UDG has both mitochondrial and nuclear isoforms, while the level of SMUG1 is not dependent on the cell cycle and is found only in the nucleus (*11*). These differences suggest distinct spatiotemporal roles for these two glycosylases.

Tremendous effort has been devoted to defining glycosylase activity using duplex DNA as the substrate (i.e., free in solution and with no DNA binding factors present). However, genomic DNA in eukaryotes is packaged into chromatin, with nucleosome core particles (NCPs) as the fundamental repeating unit. An NCP consists of 145-147 bp of duplex DNA wrapped ∼1.7 times around an octameric histone protein core, which is comprised of two H2A-H2B dimers and an $(H3\text{-}H4)_2$ tetramer. Within an NCP, there exists a two-fold axis of pseudosymmetry known as the dyad axis (*12*). The position of a nucleobase in an NCP is typically described in terms of its translational position, the displacement from the dyad axis, and its rotational position, the orientation inward towards the protein or outward towards the solution.

Due to the interaction with histones, DNA in an NCP is structurally and dynamically constrained, posing challenges to DNA-processing enzymes associated with multiple cellular processes including transcription and repair. Nucleobases facing outward are highly solution-accessible while those facing inward toward the histones are occluded and virtually solution-inaccessible. Nevertheless, the transient and spontaneous unwrapping of nucleosomal DNA can expose occluded nucleobases near the DNA entry/exit region (*13*, *14*). Several other mechanisms can actively modulate DNA accessibility in cells, including histone post-translational modifications (PTMs), chromatin remodeling, and the incorporation of histone variants into chromatin.

Histone variants are nonallelic isoforms of canonical histones that exhibit varied degrees of divergence in amino acid sequence relative to their conventional counterparts. Replacement of canonical histones with variants can confer distinct structures and dynamics and, in turn, specialized functions to variant-containing NCPs. The H2A family contains the largest number of variants. Three structural segments of these H2A variants are essential for diversifying intra- and inter-nucleosomal associations (*15*, *16*): the docking domain residing in the C-terminus, the L1 loop, and the acidic patch. One of the most extensively studied H2A variants is H2A.Z, which is found in almost all eukaryotes. Although H2A.Z is only ∼60% identical to canonical H2A, it is highly conserved among species (*15*), indicating its unique and significant function. Indeed, H2A.Z has been implicated in a multitude of biological events including transcription, double-strand break (DSB) repair, nucleotide excision repair (NER), heterochromatin silencing, chromosome segregation, and progression through the cell cycle (*17*–*19*). MacroH2A is another H2A variant of particular interest. It possesses an H2A-like histone domain connected via a lysine-rich linker to a C-terminal macro domain. In addition to inactivating X chromosomes (*20*) and orchestrating gene expression (*21*, *22*), macroH2A has been shown to function in DSB DNA damage response (*23*). Based on the fact that H2A.Z and macroH2A are involved in other DNA repair pathways, we questioned whether these two variants play a role in BER as well.

In this work, we evaluated the global profile of U excision by UDG and SMUG1 in the context of packaged DNA, using a population of NCPs that contain U lesions with a wide variety of translational and rotational positions. By substituting canonical H2A with H2A.Z or macroH2A, we investigated the impact of these two H2A variants on the initiation of BER. Further, we performed single-turnover kinetics experiments to determine UDG and SMUG1 efficiency on NCPs containing these histone variants.

Results and Discussion

Characterization of NCPs with global C to U substitution

To investigate the global profile of U removal from canonical NCPs or those containing histone H2A variants, we prepared NCPs using "Widom 601" DNA (*24*). This positioning sequence possesses high affinity for and binds the histone octamer in a single orientation (*25*). U lesions were globally incorporated into the "I strand" of Widom 601 DNA using chemical synthesis techniques to create U:G bp, mimicking the natural consequence of cytosine deamination (the full sequences of all DNA strands used in this study are shown in supplementary text and Figure S1). The global incorporation of U was achieved using a mixture of C/U building blocks during DNA synthesis with the molar ratio determined by a Poisson distribution, ensuring that 95% of the DNA contained at most one U per strand. Incubating the single-stranded DNA with UDG confirmed that the strategy provides a population of DNA where collectively each C is replaced with U (Figure S2).

NCPs were reconstituted with DNA containing global U lesions and histone octamers via salt gradient dialysis. Since homotypic H2A.Z NCPs have been determined to be enriched at active genes in *Drosophila* (*26*) and to exist exclusively (rather than heterotypic NCPs) in *Arabidopsis thaliana* (*27*), we reconstituted homotypic H2A.Z and macroH2A containing NCPs, in which both copies of canonical H2A were replaced by the variant protein. Similar to other studies that examined the influence of macroH2A incorporation on NCPs we used the histone domain of the variant (*28–31*). Formation of NCPs and their purity was evaluated by native PAGE (Figure S3). While canonical and H2A.Z NCPs migrate as a single species, macroH2A NCPs migrate as two species. A similar observation was reported previously for macroH2A NCPs (*29*). To determine if these two species arise from different translational positioning of the DNA, we performed a heat-shifting assay where NCPs were incubated at 37 °C or 55 °C (Figure S4) (*32*). No heat-induced redistribution of the NCP species was observed, indicating that the two species are thermodynamically stable under the experimental conditions with no interchange between the two species. We therefore hypothesized that macroH2A NCPs exist as two distinct populations.

Hydroxyl radical footprinting (HRF) was then utilized to establish the solution accessibility of U lesions in NCPs. Nucleobases that face outward are highly susceptible to hydroxyl radicals, resulting in strand cleavage, while nucleobases that face in toward the histone protein core are sequestered and protected from cleavage. The expected oscillatory pattern of cleavage is observed in the HRF profiles for all NCPs (Figure S5 A and B). To categorize the solution accessibility of each nucleobase, we first identified the highest HRF reactivity within a helical turn of nucleosomal DNA. The ratio of band intensity at each nucleobase position within this helical turn was then obtained by dividing the HRF value at a given position by the highest HRF reactivity. Positions with a ratio greater than 0.8, ranging between 0.8-0.2, and below 0.2 were assigned as sites that have high, intermediate, and low solution accessibility, respectively. Notably, U lesions are located at diverse translational positions and with varied levels of solution accessibility (Figure S5 C), allowing us to evaluate U removal from NCPs on a global level.

Enhanced excision of U from NCPs containing H2A variants

We next investigated U removal by UDG and SMUG1 in the context of NCPs. We used single-turnover conditions where [glycosylase]≫[substrate]. Since UDG and SMUG1 are able to excise U from duplex DNA (*33*, *34*), we included this substrate as a positive control for enzymatic activity (Figure S6 and S7). At each U site the ratio of product yield (after 60 min-reaction) in NCPs to that in duplex DNA was plotted versus nucleobase position. A ratio of 1 indicates that the lesion can be excised as efficiently in NCPs as

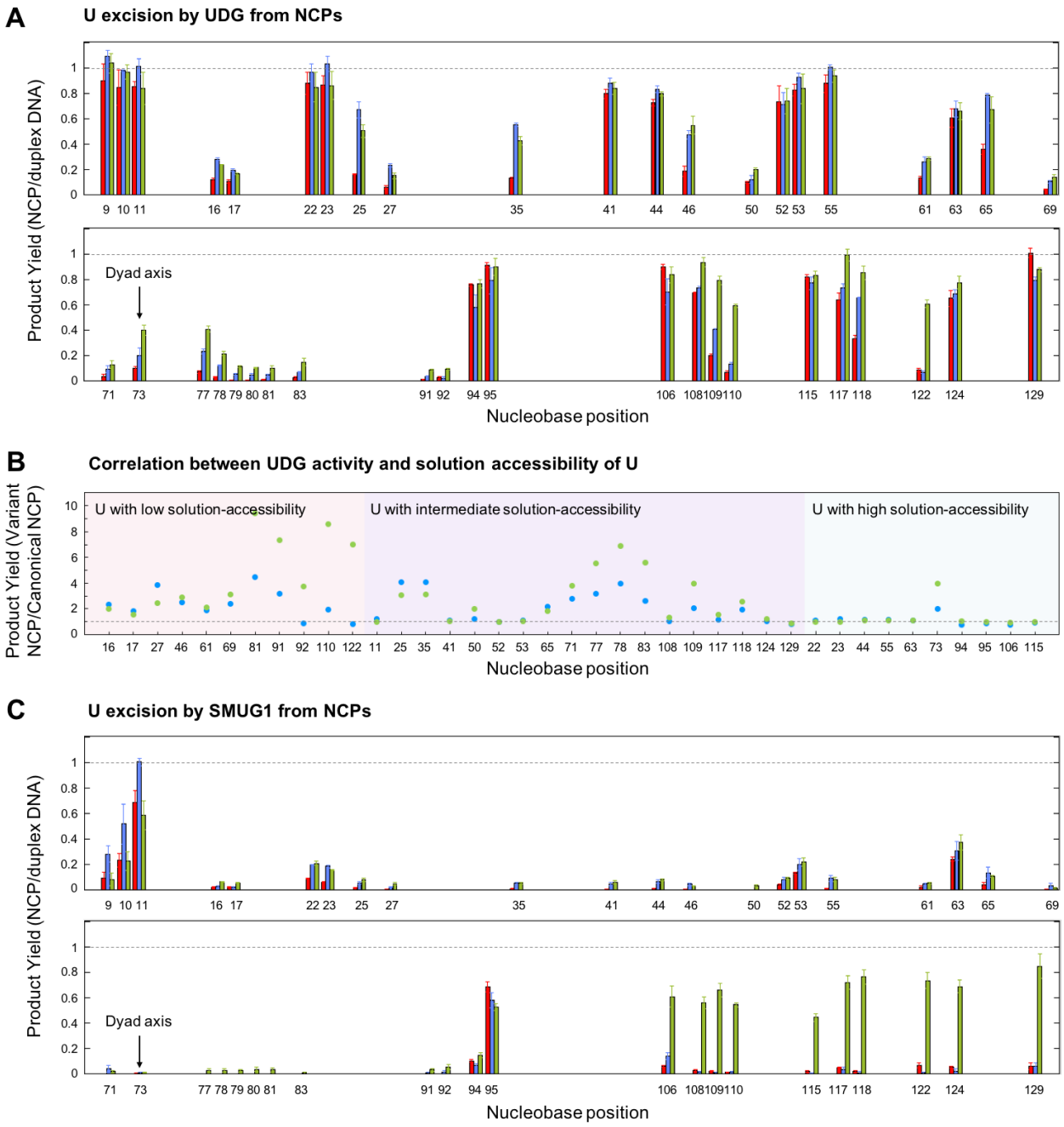

Figure 1: Excision of U from NCPs containing global C to U substitution after 60 min-incubation with glycosylases. (A) U excision initiated by UDG. At each U site the ratio of product yield in NCPs to that in duplex DNA is plotted versus nucleobase position (canonical NCP: red; H2A.Z NCP: blue; macroH2A NCP: green). The ratio of 1 is indicated as a dashed line and reflects a case where U excision from NCPs is as efficient as in duplex DNA. Position of the dyad axis is indicated by an arrow. (B) U excision initiated by UDG. U sites are re-categorized based on their solution accessibility. At each U site the ratio of product yield in H2A.Z NCPs (blue dots) or in macroH2A NCPs (green dots) to that in canonical NCPs is plotted. The ratio over 1 indicates a greater level of U excision from variant NCPs than canonical NCPs. (C) U excision initiated by SMUG1. At each U site the ratio of product yield in NCPs to that in duplex DNA is plotted versus nucleobase position (canonical NCP: red; H2A.Z NCP: blue; macroH2A NCP: green). Error bars represent the standard error (n=5).

in duplex DNA. We observed that UDG activity in canonical NCPs is largely dominated by solution accessibility of U (Figure 1A, red bars). Multiple sites with high solution accessibility, as determined by HRF, exhibit high UDG activity where ratios exceed 0.6 (sites 22, 23, 44, 55, 63, 94, 95, 106 and 115). In a similar manner, sites that face toward the histone protein core have low solution accessibility, and as expected, display minimal UDG activity with ratios below 0.2 (sites 16, 17, 27, 46, 61, 69, 81, 91, 92, 110 and 122). The region flanking the dyad axis, spanning from site 70 to site 92, is a notable exception to solution accessibility dictating glycosylase activity; excision of U by UDG is significantly inhibited regardless of solution accessibility in this region.

In the macroH2A-containing NCPs, the correlation between solution accessibility of U and UDG activity is generally retained, with some exceptions. In Figure 1B, UDG activity in variant NCPs is compared to that in canonical NCPs; a ratio of or greater than 1 indicates comparable or enhanced U excision in variant NCPs, respectively. While most highly solution-accessible U sites still exhibit high UDG reactivity, 1.5- to 10-times more product is observed at all sites with low solution accessibility and at 11/18 sites with intermediate solution accessibility compared to canonical NCPs (Figure 1B, green dots). Moreover, whereas U removal is still inhibited in the dyad region relative to the rest of the sequence, an overall increase in UDG activity is worth noting, especially at sites 73 and 77 with ratios reaching 0.4 (Figure 1A, green bars). Quite intriguingly, starting from site 108 and to the last examined lesion site 129, there is efficient U excision at all lesion sites in this region, with a remarkable increase in UDG activity at sites 109, 110 and 122, relative to canonical NCPs.

Similar to the influence exerted by macroH2A, the incorporation of H2A.Z gives rise to 2 to 5-times higher UDG activity at most lesion sites with low solution accessibility and half of the sites with intermediate solution accessibility relative to canonical NCPs (sites 25, 27, 35, 46, 65, 109, and 118) (Figure 1B, blue dots). Additionally, a small but statistically greater amount of U removal is observed at most sites in the dyad region of H2A.Z NCPs (Figure 1A, blue bars). Nevertheless, the striking enhancement in UDG activity observed for macroH2A at sites 109, 110, and 122 is not observed with H2A.Z.

Unlike UDG, SMUG1 activity is substantially suppressed along the entire sequence in canonical NCPs (Figure 1C, red bars); efficient U excision by SMUG1 is only detected at site 11, which is moderately exposed to solution and close to the DNA entry/exit region, and at site 95, which is highly solution-accessible. Of particular interest, within macroH2A NCPs restoration of glycosylase activity is manifested for SMUG1 as well in the region from site 106 to 129, revealed by the high ratios of product yield (ranging between 0.45 and 0.85) at all U sites (Figure 1C, green bars). The incorporation of H2A.Z, on the other hand, has minimal influence on U excision and nearly the same level of repair is observed for canonical and H2A.Z NCPs (Figure 1C, blue bars).

Kinetics of U excision by UDG and SMUG1 from H2A variant NCPs

To further understand the effect of H2A variants on U removal from NCPs, we performed kinetic experiments on substrates containing a single C to U substitution. Site 110 was selected for the lesion position since it is a site where both UDG and SMUG1 exhibit a drastic difference in reactivity in canonical versus H2A variant NCPs. Moreover, site 110 is in close proximity to the L1-L1′ interface of the two H2A-H2B dimers. Distinct structural properties of the L1-L1′ interface has been proposed in macroH2A and H2A.Z NCPs to confer specialized biological functions (*16*). The experiment was performed under single-turnover conditions, and the observed rate (k_{obs}) reflects the slowest step up to and including cleavage of the glycosidic bond (*35*).

Consistent with earlier reports, UDG excises U from 145 bp duplex DNA with a k_{obs} of 21 min^{-1} (Figure 2, Figure S8, Table 1) (*34*, *36*). In contrast, UDG activity is diminished in canonical and H2A.Z NCPs, as evidenced by

a maximum of 8% and 16% product yield, respectively. As site 110 exhibits low solution accessibility, this decrease in UDG reactivity in NCP is not surprising and is likely caused by steric obstruction by the protein core. In macroH2A NCPs, however, remarkable restoration of UDG activity is observed with the product yield increasing to 66%. It is notable that product yields observed in this site-specific kinetics study agree with those obtained for site 110 using the global U-containing NCPs (Figure 1A), validating the feasibility of the approach in which U removal in NCPs can be assessed both globally and quantitatively.

Interestingly, UDG exhibits two kinetic phases for all NCP substrates. While product formation for the slow phase is 150- to 500-times slower than in duplex DNA, rates of the fast phase are comparable to k_{obs} for duplex DNA, suggesting a population that is nearly as accessible as duplex. Nevertheless, since the fast phase accounts for a very small fraction of product in canonical and H2A.Z NCPs (∼3%), it is possible that the fast phase results from a small amount of duplex DNA rather than from authentic NCP substrates. However, this cannot be applicable for macroH2A NCPs, as a majority of the product (71%) in macroH2A NCPs is obtained in the fast phase, indicating a distinct population that is amenable to processing by UDG.

Compared to UDG, SMUG1 excises U from duplex DNA at a much slower rate (k_{obs} = 0.55 min^{-1}) and is significantly impaired with less than 5% product formation observed for canonical and H2A.Z NCPs. With macroH2A NCPs, a product yield of nearly 60% is observed, most of which is contributed by the fast phase (k_{obs} = 0.38 min^{-1}).

MacroH2A NCPs are a mixture of octasomes and hexasomes

We next addressed the question of why UDG and SMUG1 activities are restored in a defined region of macroH2A NCPs, sites 108-129. Since two distinct species were observed by native PAGE, we performed HRF reactions on these two species separately to investigate their

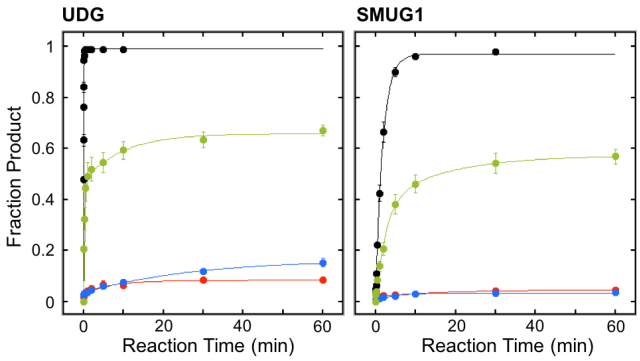

Figure 2: Single-turnover kinetics time courses of UDG and SMUG1 acting on duplex DNA and NCPs containing a single C to U substitution at site 110. Glycosylase reactions were conducted using 20 nM duplex DNA (black) or NCPs (canonical NCP: red; H2A.Z NCP: blue; macroH2A NCP: green) and 640 nM UDG or SMUG1. Lines are the best fit to the appropriate single- or double-exponential growth models. Error bars represent the standard error (n=3).

architecture (Figure 3 and Figure S9). For the faster-migrating species, which co-migrates with canonical NCPs, the oscillatory pattern of cleavage is observed along the entire length of DNA. In contrast, starting from site 115 to site 140, the slower-migrating species exhibits high susceptibility towards hydroxyl radicals irrespective of the rotational orientation relative to histones, indicating much weaker interaction or loss of contact between the DNA and the protein core. Importantly, this region is where we observed restoration of UDG and SMUG1 activity. The slower-migrating species possesses a less compact conformation, in which only ∼115 bp of DNA is tightly associated with the histone core. Notably, this observation is consistent with earlier studies of a hexasome, which lacks one copy of H2A-H2B dimer and wraps only 112 bp of DNA (*37*, *38*). Furthermore, we note that the macroH2A-H2B dimer is preferentially depleted in the area that is near the 3′ end of the I strand in the hexasomes, since this is the only region where we observed overall increased susceptibility of nucleosomal DNA towards hydroxyl radicals.

Table 1: Kinetic parameters for U excision at site 110 by UDG and SMUG1 from duplex DNA and NCPs.

Enzyme	Substrate	k_{obs}/min (%product)[1]	
		Fast phase	Slow phase
UDG	duplex DNA	21.0 ± 0.4 (99%)	
	canonical NCP	6.5 ± 2.4 (3.6%)	0.14 ± 0.04 (4.8%)
	H2A.Z NCP	16 ± 4 (3.4%)	0.037 ± 0.004 (13%)
	macroH2A NCP	6.7 ± 0.5 (47%)	0.10 ± 0.02 (19%)
SMUG1	duplex DNA	0.55 ± 0.02 (97%)	
	canonical NCP	1.4 ± 0.5 (2.0%)	0.059 ± 0.026 (2.6%)
	H2A.Z NCP	0.23 ± 0.05 (2.8%)	
	macroH2A NCP	0.38 ± 0.07 (38%)	0.061 ± 0.038 (19%)

[1] Error represents standard deviation from fitting by weighted nonlinear least-squares regression.

To confirm a portion of macroH2A NCPs forms hexasomes, we treated the NCPs with micrococcal nuclease (MNase), which preferentially digests DNA that is not closely associated with the histone core. For canonical NCPs, two distinct DNA fragments, a 128 mer and a 132 mer, were observed at high MNase concentration (Figure 4), indicating that 13-17 bp of DNA were digested at the 3′ end of the I strand, likely due to the transient unwrapping of DNA in the entry-exit region. Additionally, cleavage at sites 95, 106, and 126 was observed as these sites are highly solution-accessible. In comparison, while macroH2A NCPs are similarly accessible to MNase at sites 95, 106, 126, 128 and 132, the cleavage at sites 102, 103, and 110 is unique to macroH2A NCPs. Notably, the 110 mer is detected for macroH2A NCPs even at low MNase concentration, indicating a weak interaction between the histone core and the 35 bp of DNA at the 3′ end of the I strand. Presence of the 102 mer and 103 mer in the digested macroH2A NCPs may result from the transient interactions of nucleosomal DNA close to the DNA entry-exit region in hexasomes. These findings, in accord with the HRF results, strongly suggest that the macroH2A NCPs in our experiments contain two species: octasomes and hexasomes.

MacroH2A octasomes and hexasomes both exhibit increased accessibility to UDG and SMUG1

The activities of UDG and SMUG1 on individual macroH2A hexasome and octasome species were next examined. After incubation with UDG or SMUG1, macroH2A NCPs containing a U at site 110 were subjected to native PAGE for separating octasomes from hexasomes (Figure 5A). Given the strong product inhibition of SMUG1, a new band appeared concomitantly with disappearance of the hexasome band, likely the SMUG1-bound hexasome complex. The level of U excision from each species was then analyzed by denaturing PAGE (Figure 5B and 5C). We found that both the hexasome and the octasome species of macroH2A NCPs exhibit increased accessibility to UDG and SMUG1 relative to canonical NCPs. Moreover, while 40% and 20% product formation are observed in macroH2A octasomes with UDG and SMUG1, respectively, 80% product formation is observed in hexasomes with both glycosylases, revealing that the hexasomes are more amenable to processing by these glycosylases than the octasomes.

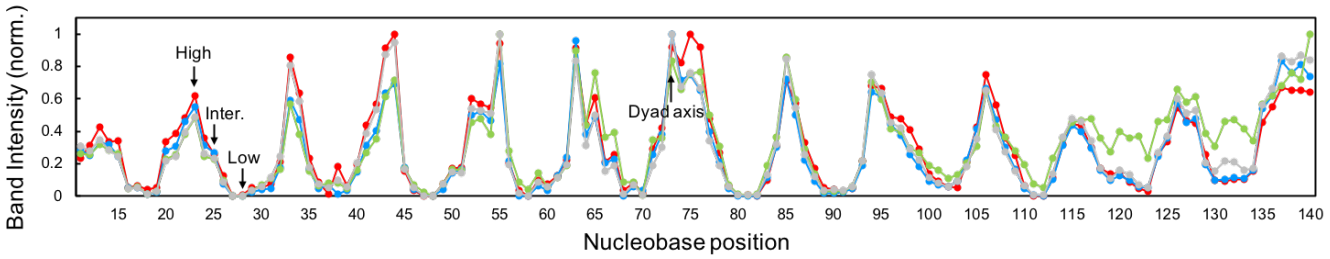

Figure 3: Hydroxyl radical footprinting of DNA in canonical and H2A variant NCPs. Band intensity at each nucleobase position on the denaturing PAGE gel (Figure S9B) was quantified and normalized, illustrating the varying solution accessibility along the sequence in each NCP sample (canonical NCP: red; H2A.Z NCP: blue; macroH2A hexasome: green; macroH2A octasome: gray). Position of the dyad axis is indicated by an arrow. Representative sites with high, intermediate (inter.) and low solution accessibility are shown.

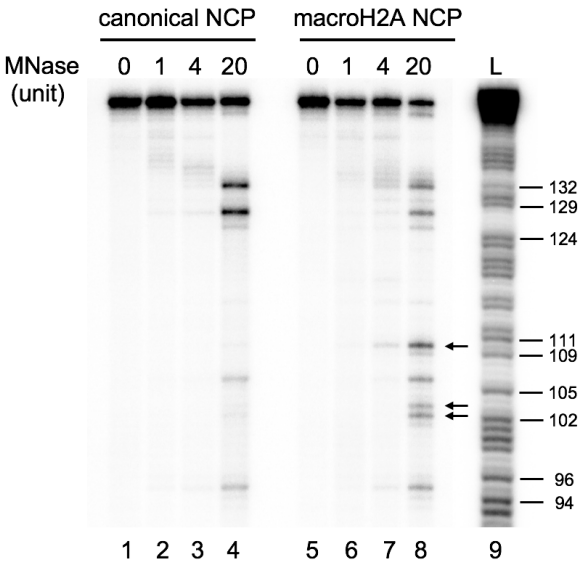

Figure 4: Micrococcal Nuclease (MNase) digestion of canonical and macroH2A NCPs. Canonical and macroH2A NCPs were treated with 1 unit (lanes 2 and 6), 4 units (lanes 3 and 7) and 20 units (lanes 4 and 8) of MNase. The negative controls in which no MNase was added are shown in lanes 1 and 5. The digestion results were resolved by denaturing PAGE. Lane 9 is a size ladder created by performing the Maxam-Gilbert sequencing reaction (A+G) on the Widom 601 J strand. Cleavage sites that are observed exclusively in macroH2A NCPs are indicated by arrows.

Mapping of U sites in H2A.Z and macroH2A NCP models

In order to investigate the impact of structural alterations in macroH2A and H2A.Z NCPs on U excision, we categorized U sites depending on the degree of increase in UDG or SMUG1 activity (more than 30% increase, 30 to 10%, less than 10%) and mapped them onto a macroH2A or H2A.Z NCP model. In the macroH2A octasome model, we note that U sites with the most dramatic increase in UDG activity cluster in three regions (Figure 6A). One region is near the docking domain at the C-terminus of macroH2A, and the other two regions are near the N-terminus of macroH2A and the L1-L1′ interface of the two macroH2A-H2B dimers. A similar clustering pattern of U sites was observed for H2A.Z octasomes (Figure S10).

Since macroH2A NCPs are a mixture of octasomes and hexasomes, we also created a macroH2A hexasome model by removing the macroH2A-H2B dimer that associates with nucleosomal DNA at the 3′ end of I strand from the octasome (Figure 6B). Earlier work demonstrated that the theoretical small-angle X-ray scattering (SAXS) curves of a canonical hexasome model constructed in this way are in good agreement with the experimental SAXS curves of the hexasomes (*37*). It is noticeable that in the macroH2A hexasome model, the region of DNA from ∼site 108 to the DNA terminus, where U sites with the largest increase in ex-

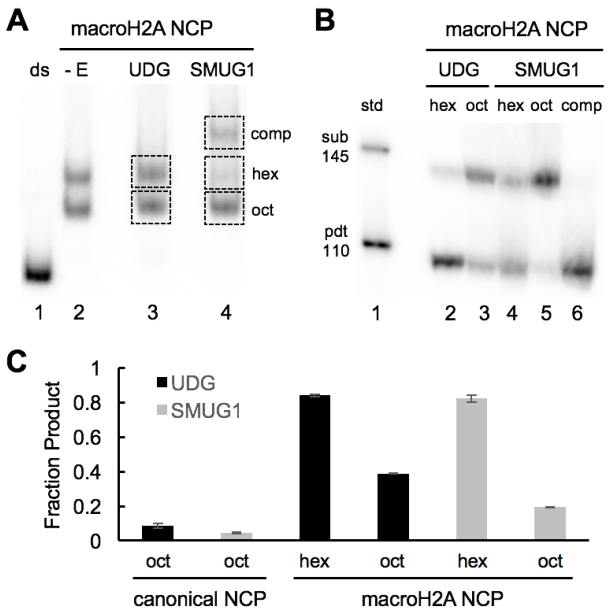

Figure 5: Differential accessibilities of U at site 110 in canonical and macroH2A NCP species to UDG and SMUG1. (A) Native PAGE analysis following the incubation of macroH2A NCPs with UDG and SMUG1. Lane 1 is a duplex DNA control. Lane 2 shows macroH2A NCPs in the absence of a glycosylase. UDG and SMUG1 treated macroH2A NCPs are shown in lanes 4 and 5, respectively; boxed bands represent the hexasomes (hex), octasomes (oct), and SMUG1-hexasome complex species (comp), and were individually excised and eluted for analysis in panel B. (B) Denaturing PAGE analysis of U excision in macroH2A hexasomes and octasomes. Lane 1 is a size marker containing a 145 mer (substrate) and 110 mer (product). Lanes 2 to 6 show the composition of each resulting eluent from the excised bands in panel A. (C) Quantitation of the denaturing PAGE gel in panel B. Fraction product with UDG or SMUG1 is shown as black and gray bars, respectively. Data for macroH2A hexasomes with SMUG1 is the weighted mean of fraction product of eluent in lanes 4 and 6 in panel B. Data for canonical NCPs is the fraction product at 60-min time point in Figure 2. Error bars represent the standard error (n=3).

cision by UDG and SMUG1 are clustered, has minimal association with the histone core.

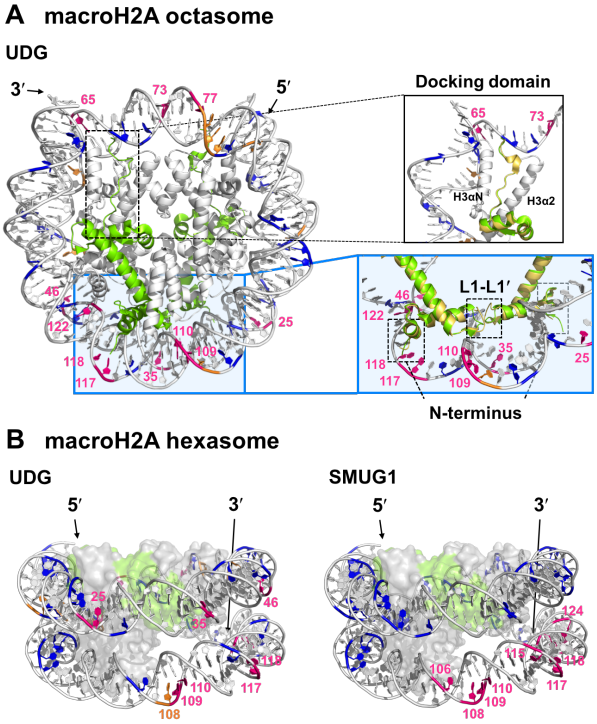

Figure 6: Model of a macroH2A (A) octasome and (B) hexasome with global C to U substitution. U sites are colored according to the level of increase in UDG or SMUG1 activity in macroH2A NCPs relative to canonical NCPs: 0 - 10% (blue), 10 - 30% (orange), and 30% and more (pink). All orange and pink sites were determined to have a p value less than 0.05 in comparison to canonical NCPs. MacroH2A is shown in green, and other histones in gray. The 5′ and 3′ ends of U-containing strand (I strand) are indicated. In the zoomed in views, canonical H2A (yellow) and macroH2A (green) are superimposed (other histones and the J strand are not included for simplification). The docking domain, L1-L1′ interface and the N-terminus of H2A/macroH2A are indicated.

Discussion

In this work, we utilized a quantitative platform for evaluating the global profile of UDG and SMUG1 repair in NCPs. In agreement with earlier work, we found that U excision by UDG from canonical NCPs is correlated with solution

accessibility of U (*39–41*), but substantially diminished in the dyad region (*42*, *43*). Indeed, a similar pattern of suppressed glycosylase activity in the dyad region has been reported for removal of 8-oxo-7,8-dihydroguanine (8-oxoG) (*36*) and 7-methyl-guanine (*44*) from NCPs via the BER pathway. This result is consistent with recent observations in cells of accumulation of oxidative and alkylation damage and high mutation frequency around the dyad axis region (*44*, *45*). Such inhibition of enzymatic activity, observed with restriction enzymes as well (*46*, *47*), may be due to the unusual helical periodicity of nuclesomal DNA in the dyad region (*48*, *49*), and the extremely low frequency of exposing nucleobases via transient unwrapping near the dyad axis (*50*).

Different observations, though, have been made in other global assessments of U excision from NCPs. We attribute these differences to the varied experimental conditions and the complexity of NCP substrates, which derives from the sequence context, base pair composition and source of histone proteins that differ in the level of PTMs. Ye and co-workers reported that, for U:A bp in Widom 601 DNA, it is predominately local DNA structure that determines U excision under multiple-turnover conditions, with rotational orientation playing a minor role at several sites (*51*). Also using U:A bp, Nilsen *et al.* observed excision of U to be only marginally reduced in NCPs assembled with 5S rDNA and chicken erythrocyte histones relative to duplex DNA, irrespective of rotational orientation (*52*).

Compared with UDG, we observed that repair initiated by SMUG1 in canonical NCPs is mostly abolished. A co-crystal structure of SMUG1 and duplex DNA shows an invasive interaction that may not be possible in NCPs (*53*). Structural constraints of nucleosomal DNA and obstruction imposed by histone proteins add other layers of difficulty for SMUG1 to process U lesions.

Due to the hindrance of canonical histones to DNA repair machinery, histone variants provide a strategy to facilitate DNA repair and maintain genomic stability (*54*). For instance, there is extensive evidence for the involvement of H2A.X, and the phosphorylated version γ-H2A.X, in response to DSB (*55*, *56*). Furthermore, the deposition of H2A.Z has been reported for remodeling chromatin architecture and recruiting machinery for DSB repair (*57*), as well as for NER (*19*). MacroH2A is also found at DSB sites and cells lacking macroH2A exhibit increased radiosensitivity (*23*). However, little is known about the potential roles of histone variants in BER. To our knowledge, one of the only two reports of histone variants in BER showed increased sensitivity of cells to methyl methanesulfonate treatment after macroH2A depletion (*23*), implying macroH2A functioning in the repair of methylated nucleobases via BER. The other one used H2A.Bbd in studies of human oxoguanine glycosylase 1 (OGG1). The authors observed minimal excision of 8-oxoG that was positioned near the dyad axis in both canonical and H2A.Bbd NCPs (*58*).

Upon replacing canonical H2A with macroH2A or H2A.Z in our experiments, we observed globally enhanced reactivity of UDG in NCPs, particularly at sites with reduced solution accessibility. Of interest, in both macroH2A and H2A.Z NCPs, sites with the largest increase in UDG efficiency are clustered and are near the docking domain, the N-terminus, and the L1 loops of the two variants. As the docking domain of the H2A variants exhibit extensive interactions with αN and α2 of H3 (Figure 6A), which associate with DNA at the DNA entry/exit region and at the dyad axis respectively, it is likely that sequence divergence in the docking domain of H2A variants strategically modulates DNA dynamics and accessibility in these regions (*16*). This effect, indeed, is also manifested in the enhanced U excision by SMUG1 in H2A.Z NCPs at the DNA entry/exit region (sites 9-11). The docking domain of H2A.Z adopts fewer hydrogen bonds with H3, leading to the destabilization of local structure. The L1 loops, being the only interface between the two H2A-H2B dimers, has been suggested to play a critical role in regulating DNA-histone binding (*59*) and the dynamics and energetics of macroH2A and H2A.Z NCPs (*28*, *60*). Consequently, struc-

tural rearrangement of the L1 loops in variant NCPs could contribute to the clustering of U sites with the largest increase in UDG activity around the L1-L1′ interface. Based on a recent study of H2A variants in *Arabidopsis thaliana* (*27*), and together with previous molecular simulations (*59*), the impact of the distinct docking domain and L1 loops of H2A variants can alter not only the structure and dynamics of individual NCP, but also inter-nucleosomal interactions. Therefore, incorporating H2A variants may be profoundly influential on the accessibility of chromatin fibers. It is also of note that due to the strong association between the Widom 601 sequence and the histone core, our observations may reflect an underestimate of the extent to which U can be repaired in other sequences; the ability of macroH2A and H2A.Z to facilitate BER may be even more dramatic than the significant effect we observed.

Another intriguing finding is the restoration of SMUG1 activity at all lesion sites in a defined region of macroH2A NCPs, where high UDG efficiency is also observed. We attribute this recovery in glycosylase activity to weaker or complete loss of DNA-histone interactions in this region, revealed by both HRF and MNase treatment. Several scenarios can result in weaker DNA-histone interplay and a less compact NCP structure, one of which is the formation of end-positioned NCPs that includes macroH2A (*61*). However, formation of the end-positioned NCPs with Widom 601 sequence requires the assistance of chromatin remodelers (*61*). Alternatively, as there has been growing evidence for preferential unwrapping of DNA from the 3′-end of the I strand in Widom 601 canonical NCP (*62*–*64*), asymmetric unwrapping can be another possibility. Nevertheless, rates of lesion site exposure induced by unwrapping alone are too low to account for observed rates of U excision at site 110 (*50*, *65*). Therefore, it is mostly likely that the formation of macroH2A hexasomes contributes to the restoration of glycosylase activity in the region 35-40 bp from the 3′-end of the I strand, and this contribution could be amplified by synergistic asymmetric unwrapping occurring within the hexasomes.

In fact, it has been reported that hexasomes can concomitantly form with octasomes during canonical NCP reconstitution (*66*), and a macroH2A hexasome species was proposed to have been observed (*29*). Intriguingly, we note that the macroH2A hexasomes appear to lack exclusively one copy of the macroH2A-H2B dimer at the 3′-end of the I strand, where the asymmetrical unwrapping of nucleosomal DNA in Widom 601 canonical NCPs is thermodynamically favored (*62*, *63*, *67*). Previous biochemical experiments indicate that macroH2A octamers are less sensitive to the decreased salt concentration and undergo a peculiar dissociation pathway during reconstitution (*29*). The distinct property of macroH2A octamers makes it possible that an incompletely dissociated species, the hexamers, are deposited onto DNA, and the more flexible 5′-end of the I strand preferentially binds with the hexamers. Alternatively, as the formation of canonical hexasomes *in vitro* is reported to be guided by asymmetric unwrapping (*64*), macroH2A octasomes may have a higher probability than canonical octasomes to release a macroH2A-H2B dimer at the 3′-end of the I strand during reconstitution. Given its distinct structure and dynamics, canonical hexasomes have emerged as an intermediate for modulating chromatin architecture and DNA accessibility during replication, transcription, and DNA repair (*68*–*73*). Notably, the finding of histone chaperone FACT, which promotes the RNA polymerase II-dependent H2A-H2B dimer eviction (*74*), to co-localize with OGG1 at damage sites may imply the involvement of the hexasomes in BER (*42*).

In our kinetic experiments, we observed biphasic kinetics in most NCPs with UDG and SMUG1. The biphasic kinetics have been reported previously for other glycosylases on NCPs (*34*, *51*, *75*). Interestingly, k_{obs} of the fast phase observed with NCPs is comparable to that of duplex DNA, indicating a substrate population that is nearly as accessible as duplex. Although the small amount of U excision ($\sim$3%) in the fast phase may derive from duplex DNA, native PAGE demonstrates that NCP samples remain intact after UDG and SMUG1 reactions (data not shown). Furthermore, single molecule FRET studies revealed

the existence of an open state of NCPs, populated 0.2-3% under physiological conditions (*76*), that may possess more accessible DNA and explain the fast phase observed with canonical and H2A.Z NCPs. In contrast, ∼50% and 40% of U excision were obtained in the fast phase with UDG and SMUG1, respectively, in macroH2A NCPs. We attribute this increase mostly to the dramatically enhanced DNA accessibility caused by the macroH2A hexasomes.

U excision in the slow phase of NCPs, on the other hand, is ∼200-times and ∼10-times slower with UDG and SMUG1, respectively, than in duplex DNA, suggesting a population of NCPs that is comparatively refractory to processing by the glycosylases. We note that while rates of the fast phase in NCPs are dramatically different for UDG and SMUG1, rates of the slow phase are relatively similar, perhaps suggesting that the NCP population accounting for the slow phase undergoes a rate-limiting structural alteration(s) to expose the lesion site or adopt a conformation permissive for repair. In comparison, NCPs in the fast phase may have the same rate-limiting step as duplex DNA since their rates are comparable under single-turnover conditions, and the rate-limiting step is determined by mechanisms unique to UDG and SMUG1, rather than by NCP conformational change(s).

Although exchanging canonical H2A with macroH2A or H2A.Z can modulate the structure and dynamics of NCPs and enhance the efficiency of BER, coupling the incorporation of histone variants with other cellular factors, such as chromatin remodelers and/or histone PTMs, could provide additional and more versatile strategies for regulating DNA accessibility and maintaining genomic integrity. Indeed, H2A.Z sumoylation has been suggested to play a role in DSB repair (*77*), and acetylated H3.3/H2A.Z hybrid nucleosomes are known to be enriched at the transcription start sites of active genes (*78*, *79*). Moreover, the C-terminal macro domain of macroH2A is capable of interacting with histone deactylases (*28*) and binding nicotinamide adenine dinucleotide metabolites (*80*, *81*), implying its diverse role in biological events. Taken together, given the complexity of chromatin, elaborate mechanisms have evolved to balance DNA accessibility and genome stability for a multitude of biological processes, such as replication, transcription, and repair. Our study demonstrates the enhancement of U excision in NCPs containing the H2A variants H2A.Z and macroH2A. Further studies with additional cellular factors will reveal the extent to which they modulate the influence of histone variants on BER.

Materials and Methods

Detailed methods are described in the Supporting Information.

Supporting information

DNA sequences, Figure S1-S10, and materials and methods.

Acknowledgement

This work was supported by National Science Foundation (MCB-1817417). The authors thank K. Luger (University of Colorado Boulder) for providing the expression plasmid for histone domain of human macroH2A, and J. Huang for optimizing the protocol for canonical histone purification. We thank members of the Delaney laboratory for helpful discussion.

References

1. Dizdaroglu, M. (2015) Oxidatively induced DNA damage and its repair in cancer. *Mutat. Res. Rev. Mutat. Res. 763*, 212–245.

2. David, S. S., and Williams, S. D. (1998) Chemistry of glycosylases and endonucleases involved in base-excision repair. *Chem. Rev. 98*, 1221–1262.

3. Schermerhorn, K. M., and Delaney, S. (2014) A Chemical and Kinetic Perspective on Base Excision Repair of DNA. *Acc. Chem. Res. 47*, 1238–1246.

4. Lindahl, T. (1993) Instability and decay of the primary structure of DNA. *Nature 362*, 709–715.

5. Nilsen, H., Haushalter, K. A., Robins, P., Barnes, D. E., Verdine, G. L., and Lindahl, T. (2001) Excision of deaminated cytosine from the vertebrate genome: role of the SMUG1 uracil-DNA glycosylase. *EMBO J. 20*, 4278–4286.

6. Kavli, B., Sundheim, O., Akbari, M., Otterlei, M., Nilsen, H., Skorpen, F., Aas, P. A., Hagen, L., Krokan, H. E., and Slupphaug, G. (2002) hUNG2 is the major repair enzyme for removal of uracil from U: A matches, U: G mismatches and U in single stranded DNA, with hSMUG1 as a broad specificity backup. *J. Biol. Chem. 277*, 39926–39936.

7. An, Q., Robins, P., Lindahl, T., and Barnes, D. E. (2005) C $\rightarrow$ T mutagenesis and γ-radiation sensitivity due to deficiency in the Smug1 and Ung DNA glycosylases. *EMBO J. 24*, 2205–2213.

8. Alsøe, L., Sarno, A., Carracedo, S., Domanska, D., Dingler, F., Lirussi, L., Sen-Gupta, T., Tekin, N. B., Jobert, L., Alexandrov, L. B., Galashevskaya, A., Rada, C., Sandve, G. K., Rognes, T., Krokan, H. E., and Nilsen, H. (2017) Uracil Accumulation and Mutagenesis Dominated by Cytosine Deamination in CpG Dinucleotides in Mice Lacking UNG and SMUG1. *Sci. Rep. 7*.

9. Greenman, C., Stephens, P., Smith, R., Dalgliesh, G. L., Hunter, C., Bignell, G., Davies, H., Teague, J., Butler, A., Stevens, C., Edkins, S., O'Meara, S., Vastrik, I., Schmidt, E. E., Avis, T., Barthorpe, S., Bhamra, G., Buck, G., Choudhury, B., Clements, J., Cole, J., Dicks, E., Forbes, S., Gray, K., Halliday, K., Harrison, R., Hills, K., Hinton, J., Jenkinson, A., Jones, D., Menzies, A., Mironenko, T., Perry, J., Raine, K., Richardson, D., Shepherd, R., Small, A., Tofts, C., Varian, J., Webb, T., West, S., Widaa, S., Yates, A., Cahill, D. P., Louis, D. N., Goldstraw, P., Nicholson, A. G., Brasseur, F., Looijenga, L., Weber, B. L., Chiew, Y.-E., DeFazio, A., Greaves, M. F., Green, A. R., Campbell, P., Birney, E., Easton, D. F., Chenevix-Trench, G., Tan, M.-H., Khoo, S. K., Teh, B. T., Yuen, S. T., Leung, S. Y., Wooster, R., Futreal, P. A., and Stratton, M. R. (2007) Patterns of somatic mutation in human cancer genomes. *Nature 446*, 153–158.

10. Kemmerich, K., Dingler, F. A., Rada, C., and Neuberger, M. S. (2012) Germline ablation of SMUG1 DNA glycosylase causes loss of 5-hydroxymethyluracil-and UNG-backup uracil-excision activities and increases cancer predisposition of Ung-/-Msh2-/- mice. *Nucleic Acids Res. 40*, 6016–6025.

11. Pettersen, H. S., Sundheim, O., Gilljam, K. M., Slupphaug, G., Krokan, H. E., and Kavli, B. (2007) Uracil DNA glycosylases SMUG1 and UNG2 coordinate the initial steps of base excision repair by distinct mechanisms. *Nucleic Acids Res. 35*, 3879–3892.

12. Luger, K., Mäder, A. W., Richmond, R. K., Sargent, D. F., and Richmond, T. J. (1997) Crystal structure of the nucleosome core particle at 2.8 Å resolution. *Nature 389*, 251–260.

13. Li, G., Levitus, M., Bustamante, C., and Widom, J. (2005) Rapid spontaneous accessibility of nucleosomal DNA. *Nat. Struct. Mol. Biol. 12*, 46–53.

14. Wei, S., Falk, S. J., Black, B. E., and Lee, T.-H. (2015) A novel hybrid single molecule approach reveals spontaneous DNA motion in the nucleosome. *Nucleic Acids Res. 43*, e111.

15. Malik, H. S., and Henikoff, S. (2003) Phylogenomics of the nucleosome. *Nat. Struct. Mol. Biol. 10*, 882–891.

16. Bönisch, C., and Hake, S. B. (2012) Histone H2A variants in nucleosomes and chromatin: more or less stable? *Nucleic Acids Res. 40*, 10719–10741.

17. Zlatanova, J., and Thakar, A. (2008) H2A.Z: view from the top. *Structure 16*, 166–179.

18. Billon, P., and Côté, J. (2012) Precise deposition of histone H2A.Z in chromatin for genome expression and maintenance. *Biochim. Biophys. Acta 1819*, 290–302.

19. Yu, Y., Deng, Y., Reed, S. H., Millar, C. B., and Waters, R. (2013) Histone variant Htz1 promotes histone H3 acetylation to enhance nucleotide excision repair in Htz1 nucleosomes. *Nucleic Acids Res. 41*, 9006–9019.

20. Costanzi, C., and Pehrson, J. R. (1998) Histone macroH2A1 is concentrated in the inactive X chromosome of female mammals. *Nature 393*, 599–601.

21. Chen, H., Ruiz, P. D., Novikov, L., Casill, A. D., Park, J. W., and Gamble, M. J. (2014) MacroH2A1.1 and PARP-1 cooperate to regulate transcription by promoting CBP-mediated H2B acetylation. *Nat. Struct. Mol. Biol. 21*, 981–989.

22. Lavigne, M. D., Vatsellas, G., Polyzos, A., Mantouvalou, E., Sianidis, G., Maraziotis, I., Agelopoulos, M., and Thanos, D. (2015) Composite macroH2A/NRF-1 nucleosomes suppress noise and generate robustness in gene expression. *Cell Rep. 11*, 1090–1101.

23. Xu, C., Xu, Y., Gursoy-Yuzugullu, O., and Price, B. D. (2012) The histone variant macroH2A1.1 is recruited to DSBs through a mechanism involving PARP1. *FEBS Lett. 586*, 3920–3925.

24. Lowary, P. T., and Widom, J. (1998) New DNA sequence rules for high affinity binding to histone octamer and sequence-directed nucleosome positioning. *J. Mol. Biol. 276*, 19–42.

25. Chua, E. Y. D., Vasudevan, D., Davey, G. E., Wu, B., and Davey, C. A. (2012) The mechanics behind DNA sequence-dependent properties of the nucleosome. *Nucleic Acids Res. 40*, 6338–6352.

26. Weber, C. M., Henikoff, J. G., and Henikoff, S. (2010) H2A.Z nucleosomes enriched over active genes are homotypic. *Nat. Struct. Mol. Biol. 17*, 1500–1507.

27. Osakabe, A., Lorković, Z. J., Kobayashi, W., Tachiwana, H., Yelagandula, R., Kurumizaka, H., and Berger, F. (2018) Histone H2A variants confer specific properties to nucleosomes and impact on chromatin accessibility. *Nucleic Acids Res. 46*, 7675–7685.

28. Chakravarthy, S., Gundimella, S. K. Y., Caron, C., Perche, P.-Y., Pehrson, J. R., Khochbin, S., and Luger, K. (2005) Structural Characterization of the Histone Variant macroH2A. *Mol. Cell. Biol. 25*, 7616–7624.

29. Chakravarthy, S., and Luger, K. (2006) The Histone Variant Macro-H2A Preferentially Forms "Hybrid Nucleosomes". *J. Biol. Chem. 281*, 25522–25531.

30. Chang, E. Y., Ferreira, H., Somers, J., Nusinow, D. A., Owen-Hughes, T., and Narlikar, G. J. (2008) MacroH2A Allows ATP-Dependent Chromatin Remodeling by SWI/SNF and ACF Complexes but Specifically Reduces Recruitment of SWI/SNF. *Biochemistry 47*, 13726–13732.

31. Angelov, D., Molla, A., Perche, P.-Y., Hans, F., Côté, J., Khochbin, S., Bouvet, P., and Dimitrov, S. (2003) The histone variant macroH2A interferes with transcription factor binding and SWI/SNF nucleosome remodeling. *Mol. Cell 11*, 1033–1041.

32. Dyer, P. N., Edayathumangalam, R. S., White, C. L., Bao, Y., Chakravarthy, S., Muthurajan, U. M., and Luger, K. (2004)

Reconstitution of nucleosome core particles from recombinant histones and DNA. *Methods Enzymol. 375*, 23–44.

33. Darwanto, A., Theruvathu, J. A., Sowers, J. L., Rogstad, D. K., Pascal, T., Goddard, W., and Sowers, L. C. (2009) Mechanisms of Base Selection by Human Single-strand Selective Monofunctional Uracil-DNA Glycosylase. *J. Biol. Chem. 284*, 15835–15846.

34. Olmon, E. D., and Delaney, S. (2017) Differential ability of five DNA glycosylases to recognize and repair damage on nucleosomal DNA. *ACS Chem. Biol. 12*, 692–701.

35. Porello, S. L., Leyes, A. E., and David, S. S. (1998) Single-turnover and pre-steady-state kinetics of the reaction of the adenine glycosylase MutY with mismatch-containing DNA substrates. *Biochemistry 37*, 14756–14764.

36. Bilotti, K., Tarantino, M. E., and Delaney, S. (2018) Human Oxoguanine Glycosylase 1 Removes Solution Accessible 8-Oxo-7,8-dihydroguanine Lesions from Globally Substituted Nucleosomes Except in the Dyad Region. *Biochemistry 57*, 1436–1439.

37. Arimura, Y., Tachiwana, H., Oda, T., Sato, M., and Kurumizaka, H. (2012) Structural Analysis of the Hexasome, Lacking One Histone H2A/H2B Dimer from the Conventional Nucleosome. *Biochemistry 51*, 3302–3309.

38. Kato, D., Osakabe, A., Arimura, Y., Mizukami, Y., Horikoshi, N., Saikusa, K., Akashi, S., Nishimura, Y., Park, S.-Y., and Nogami, J. (2017) Crystal structure of the overlapping dinucleosome composed of hexasome and octasome. *Science 356*, 205–208.

39. Hinz, J. M., Rodriguez, Y., and Smerdon, M. J. (2010) Rotational dynamics of DNA on the nucleosome surface markedly impact accessibility to a DNA repair enzyme. *Proc. Natl. Acad. Sci. U.S.A. 107*, 4646–4651.

40. Beard, B. C., Wilson, S. H., and Smerdon, M. J. (2003) Suppressed catalytic activity of base excision repair enzymes on rotationally positioned uracil in nucleosomes. *Proc. Natl. Acad. Sci. U.S.A. 100*, 7465–7470.

41. Rodriguez, Y., and Smerdon, M. J. (2013) The Structural Location of DNA Lesions in Nucleosome Core Particles Differentially Influence Accessibility of Base Excision Repair Enzymes. *J. Biol. Chem. 288*, 13863–13875.

42. Charles Richard, J. L., Shukla, M. S., Menoni, H., Ouararhni, K., Lone, I. N., Roulland, Y., Papin, C., Ben Simon, E., Kundu, T., Hamiche, A., Angelov, D., and Dimitrov, S. (2016) FACT Assists Base Excision Repair by Boosting the Remodeling Activity of RSC. *PLoS Genet. 12*, e1006221.

43. Cole, H. A., Tabor-Godwin, J. M., and Hayes, J. J. (2010) Uracil DNA Glycosylase Activity on Nucleosomal DNA depends on Rotational Orientation of Targets. *J. Biol. Chem. 285*, 2876–2885.

44. Mao, P., Brown, A. J., Malc, E. P., Mieczkowski, P. A., Smerdon, M. J., Roberts, S. A., and Wyrick, J. J. (2017) Genome-wide maps of alkylation damage, repair, and mutagenesis in yeast reveal mechanisms of mutational heterogeneity. *Genome Res. 27*, 1674–1684.

45. Wu, J., McKeague, M., and Sturla, S. J. (2018) Nucleotide-resolution genome-wide mapping of oxidative DNA damage by click-code-seq. *J. Am. Chem. Soc. 140*, 9783–9787.

46. Anderson, J., and Widom, J. (2000) Sequence and position-dependence of the equilibrium accessibility of nucleosomal DNA target sites. *J. Mol. Biol. 296*, 979–987.

47. Polach, K., and Widom, J. (1995) Mechanism of Protein Access to Specific DNA

Sequences in Chromatin: A Dynamic Equilibrium Model for Gene Regulation. *J. Mol. Biol. 254*, 130–149.

48. Hayes, J. J., Tullius, T. D., and Wolffe, A. P. (1990) The structure of DNA in a nucleosome. *Proc. Natl. Acad. Sci. U.S.A. 87*, 7405–7409.

49. Hayes, J. J., Clark, D. J., and Wolffe, A. P. (1991) Histone contributions to the structure of DNA in the nucleosome. *Proc. Natl. Acad. Sci. U.S.A. 88*, 6829–6833.

50. Tims, H. S., Gurunathan, K., Levitus, M., and Widom, J. (2011) Dynamics of Nucleosome Invasion by DNA Binding Proteins. *J. Mol. Biol. 411*, 430–448.

51. Ye, Y., Stahley, M. R., Xu, J., Friedman, J. I., Sun, Y., McKnight, J. N., Gray, J. J., Bowman, G. D., and Stivers, J. T. (2012) Enzymatic Excision of Uracil Residues in Nucleosomes Depends on the Local DNA Structure and Dynamics. *Biochemistry 51*, 6028–6038.

52. Nilsen, H., Lindahl, T., and Verreault, A. (2002) DNA base excision repair of uracil residues in reconstituted nucleosome core particles. *EMBO J. 21*, 5943–5952.

53. Wibley, J. E., Waters, T. R., Haushalter, K., Verdine, G. L., and Pearl, L. H. (2003) Structure and specificity of the vertebrate anti-mutator uracil-DNA glycosylase SMUG1. *Mol. Cell 11*, 1647–1659.

54. Volle, C., and Dalal, Y. (2014) Histone variants: the tricksters of the chromatin world. *Curr. Opin. Genet. Dev. 25*, 8–14.

55. Rogakou, E. P., Boon, C., Redon, C., and Bonner, W. M. (1999) Megabase Chromatin Domains Involved in DNA Double-Strand Breaks in Vivo. *J. Cell Biol. 146*, 905–916.

56. Kinner, A., Wu, W., Staudt, C., and Iliakis, G. (2008) γ-H2AX in recognition and signaling of DNA double-strand breaks in the context of chromatin. *Nucleic Acids Res. 36*, 5678–5694.

57. Xu, Y., Ayrapetov, M. K., Xu, C., Gursoy-Yuzugullu, O., Hu, Y., and Price, B. D. (2012) Histone H2A.Z Controls a Critical Chromatin Remodeling Step Required for DNA Double-Strand Break Repair. *Mol. Cell 48*, 723–733.

58. Menoni, H., Gasparutto, D., Hamiche, A., Cadet, J., Dimitrov, S., Bouvet, P., and Angelov, D. (2007) ATP-Dependent Chromatin Remodeling Is Required for Base Excision Repair in Conventional but Not in Variant H2A.Bbd Nucleosomes. *Mol. Cell. Biol. 27*, 5949–5956.

59. Bowerman, S., and Wereszczynski, J. (2016) Effects of MacroH2A and H2A.Z on Nucleosome Dynamics as Elucidated by Molecular Dynamics Simulations. *Biophys. J. 110*, 327–337.

60. Suto, R. K., Clarkson, M. J., Tremethick, D. J., and Luger, K. (2000) Crystal structure of a nucleosome core particle containing the variant histone H2A.Z. *Nat. Struct. Biol. 7*, 1121–1124.

61. Shukla, M. S., Syed, S. H., Montel, F., Faivre-Moskalenko, C., Bednar, J., Travers, A., Angelov, D., and Dimitrov, S. (2010) Remosomes: RSC generated non-mobilized particles with approximately 180 bp DNA loosely associated with the histone octamer. *Proc. Natl. Acad. Sci. U.S.A. 107*, 1936–1941.

62. Ngo, T. T., Zhang, Q., Zhou, R., Yodh, J. G., and Ha, T. (2015) Asymmetric Unwrapping of Nucleosomes under Tension Directed by DNA Local Flexibility. *Cell 160*, 1135–1144.

63. de Bruin, L., Tompitak, M., Eslami-Mossallam, B., and Schiessel, H. (2016) Why Do Nucleosomes Unwrap Asymmetrically? *J. Phys. Chem. B 120*, 5855–5863.

64. Chen, Y., Tokuda, J. M., Topping, T., Meisburger, S. P., Pabit, S. A., Gloss, L. M., and Pollack, L. (2017) Asymmetric unwrapping of nucleosomal

DNA propagates asymmetric opening and dissociation of the histone core. *Proc. Natl. Acad. Sci. U.S.A. 114*, 334–339.

65. Maher, R. L., Prasad, A., Rizvanova, O., Wallace, S. S., and Pederson, D. S. (2013) Contribution of DNA unwrapping from histone octamers to the repair of oxidatively damaged DNA in nucleosomes. *DNA Repair (Amst). 12*, 964–971.

66. Azegami, N., Saikusa, K., Todokoro, Y., Nagadoi, A., Kurumizaka, H., Nishimura, Y., and Akashi, S. (2013) Conclusive Evidence of the Reconstituted Hexasome Proven by Native Mass Spectrometry. *Biochemistry 52*, 5155–5157.

67. Bilokapic, S., Strauss, M., and Halic, M. (2018) Histone octamer rearranges to adapt to DNA unwrapping. *Nat. Struct. Mol. Biol. 25*, 101–108.

68. Zlatanova, J., Bishop, T. C., Victor, J.-M., Jackson, V., and van Holde, K. (2009) The Nucleosome Family: dynamic and growing. *Structure 17*, 160–171.

69. Groth, A., Rocha, W., Verreault, A., and Almouzni, G. (2007) Chromatin Challenges during DNA Replication and Repair. *Cell 128*, 721–733.

70. Heo, K., Kim, H., Choi, S. H., Choi, J., Kim, K., Gu, J., Lieber, M. R., Yang, A. S., and An, W. (2008) FACT-Mediated Exchange of histone Variant H2AX Regulated by Phosphorylation of H2AX and ADP-Ribosylation of Spt16. *Mol. Cell 30*, 86–97.

71. Mizuguchi, G., Shen, X., Landry, J., Wu, W.-H., Sen, S., and Wu, C. (2004) ATP-driven exchange of histone H2AZ variant catalyzed by SWR1 chromatin remodeling complex. *Science 303*, 343–348.

72. Luk, E., Ranjan, A., FitzGerald, P. C., Mizuguchi, G., Huang, Y., Wei, D., and Wu, C. (2010) Stepwise histone replacement by SWR1 requires dual activation with histone H2A.Z and canonical nucleosome. *Cell 143*, 725–736.

73. Levchenko, V., and Jackson, V. (2004) Histone release during transcription: NAP1 forms a complex with H2A and H2B and facilitates a topologically dependent release of H3 and H4 from the nucleosome. *Biochemistry 43*, 2359–2372.

74. Belotserkovskaya, R., Oh, S., Bondarenko, V. A., Orphanides, G., Studitsky, V. M., and Reinberg, D. (2003) FACT facilitates transcription-dependent nucleosome alteration. *Science 301*, 1090–1093.

75. Bilotti, K., Kennedy, E. E., Li, C., and Delaney, S. (2017) Human OGG1 activity in nucleosomes is facilitated by transient unwrapping of DNA and is influenced by the local histone environment. *DNA Repair (Amst). 59*, 1–8.

76. Böhm, V., Hieb, A. R., Andrews, A. J., Gansen, A., Rocker, A., Tóth, K., Luger, K., and Langowski, J. (2011) Nucleosome accessibility governed by the dimer/tetramer interface. *Nucleic Acids Res. 39*, 3093–3102.

77. Kalocsay, M., Hiller, N. J., and Jentsch, S. (2009) Chromosome-wide Rad51 spreading and SUMO-H2A.Z-dependent chromosome fixation in response to a persistent DNA double-strand break. *Mol. Cell 33*, 335–343.

78. Jin, C., Zang, C., Wei, G., Cui, K., Peng, W., Zhao, K., and Felsenfeld, G. (2009) H3.3/H2A.Z double variantâĂŞcontaining nucleosomes mark 'nucleosome-free regions' of active promoters and other regulatory regions. *Nature Genet. 41*, 941–945.

79. Valdés-Mora, F., Song, J. Z., Statham, A. L., Strbenac, D., Robinson, M. D., Nair, S. S., Patterson, K. I., Tremethick, D. J., Stirzaker, C., and Clark, S. J. (2012) Acetylation of H2A.Z is a key epigenetic modification associated with gene deregulation and epigenetic remodeling in cancer. *Genome Res. 22*, 307–321.

80. Timinszky, G., Till, S., Hassa, P. O., Hothorn, M., Kustatscher, G., Nijmeijer, B., Colombelli, J., Altmeyer, M., Stelzer, E. H. K., Scheffzek, K., Hottiger, M. O., and Ladurner, A. G. (2009) A macrodomain-containing histone rearranges chromatin upon sensing PARP1 activation. *Nat. Struct. Mol. Biol. 16*, 923–929.

81. Kustatscher, G., Hothorn, M., Pugieux, C., Scheffzek, K., and Ladurner, A. G. (2005) Splicing regulates NAD metabolite binding to histone macroH2A. *Nat. Struct. Mol. Biol. 12*, 624–625.

Graphical TOC Entry